Lanthanide-Doped Nanoprobes as Orthogonal NIR-II Fluorescence Channels for In Vivo Information Storage

Wang, Xiaolu; Jia, Qi; Ma, Liyi; Zhai, Xuejiao; Liu, Yuxin; Liao, Xianquan; Zhou, Jing

DOI
10.1021/acsanm.2c03951

Publication date
2022

Document Version
Final published version

Published in
ACS Applied Nano Materials

ACS APPLIED NANO MATERIALS

www.acsanm.org Article

Lanthanide-Doped Nanoprobes as Orthogonal NIR-II Fluorescence Channels for In Vivo Information Storage

Xiaolu Wang,[⊥] Qi Jia,[⊥] Liyi Ma, Xuejiao Zhai, Yuxin Liu, Xianquan Liao, and Jing Zhou*

Cite This: https://doi.org/10.1021/acsanm.2c03951 Read Online

ACCESS | Metrics & More | Article Recommendations | Supporting Information

ABSTRACT: Information storage in vivo will lead to next-generation identification and security authentication. Here, an information storage method was proposed for in vivo application by using a pair of lanthanide-doped nanoprobes (NdNPs and ErNPs) with orthogonal emissions in the second near-infrared window. The information is stored in different fluorescence channels separately, while the selective readout could be realized by simply manipulating excitation wavelengths. The small-animal experiments primarily confirm the applicability of this method in vivo. The binary numbers ″1″ and ″0″ are implanted under the mice's skin, and the corresponding signals ″on″ and ″off″ can be collected by charge-coupled devices under different laser filter combinations. The design of lanthanide-doped probes with the nanoscale features and orthogonal emissions is expected to provide a new strategy for information storage in vivo. The lanthanide materials with excellent down-conversion near-infrared fluorescence performance have shown great application potential in the field of photonics.

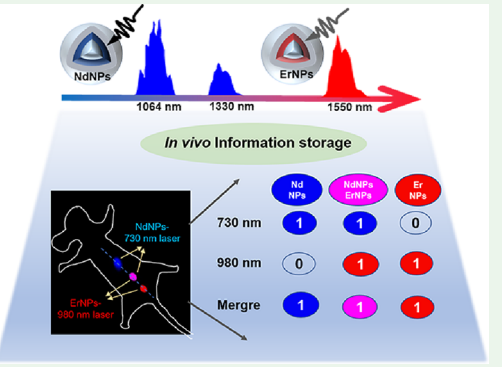

KEYWORDS: *rare earth-based nanoparticles, second near-infrared window, orthogonal, multichannel imaging, information storage*

INTRODUCTION

Rapid identification and security authentication have drawn great attention in the field of photonics.[1−4] Storing information in vivo is considered one of the attractive solutions to this technical requirement as it is direct and applicable.[5] By integrating and transforming complex information into physical signals (e.g., magnetic and optical signals), it is possible to read out the information of interest from living biosystems directly.[6−14] Fluorescence imaging is a mature and noninvasive technique for signal readout,[15−17] which has shown its potential in information storage in vitro and could be useful for in vivo applications.[18−21]

Due to their superior photostability and biocompatibility,[22−26] lanthanide-doped nanoprobes are widely used in bioimaging.[27−30] Therefore, the lanthanide-doped nanoprobes are outstanding candidates for fluorescence-based in vivo information storage.[20,31,32] It is notable that, contributing to the unique 4f−4f electron layers of lanthanide ions, the lanthanide-doped nanoprobes exhibit line-shaped absorbance and emission bands with narrow half-width peaks and good orthogonality, which would further allow us to establish multichannel information storage for different purposes.[33−37] Conventionally, the selective separation of emissions depends on the use of filters or their lifetime, which requires either complex operation or expensive instruments, thereby being difficult for practical transformation.[38−40] Benefiting from the line-shaped absorbance bands, it is possible to selectively excite lanthanide ions with specific excitation, avoiding the use of extra accessional equipment, which would be facile for operation and of great interest to actual practice. Compared with traditional NIR-I or visible light, NIR-II fluorescence has higher tissue penetration depth and lower tissue absorption and scattering.[20,41] Therefore, the NIR-II luminescence has superiority in the field of information storage *in vivo*.

Here, a pair of lanthanide-doped nanoprobes, $NaYF_4$:Gd@$NaYF_4$:Nd@$NaYF_4$ (NdNPs) and $NaYF_4$:Gd@$NaErF_4$@$NaYF_4$ (ErNPs), was constructed as fluorescent labels of information. The lanthanide-doped probes with the nanoscale features (∼27 nm) and NIR-II orthogonal emissions for information storage were investigated *in vitro* and *in vivo*.

RESULTS AND DISCUSSION

$NaYF_4$:Gd@$NaYF_4$:Nd@$NaYF_4$ (NdNPs) and $NaYF_4$:Gd@$NaErF_4$@$NaYF_4$ (ErNPs) are synthesized by a typical solvothermal method.[41−43] The transmission electron microscope images indicate that the as-prepared NdNPs and ErNPs have uniform spherical morphology with a similar size

Received: September 6, 2022
Accepted: October 21, 2022

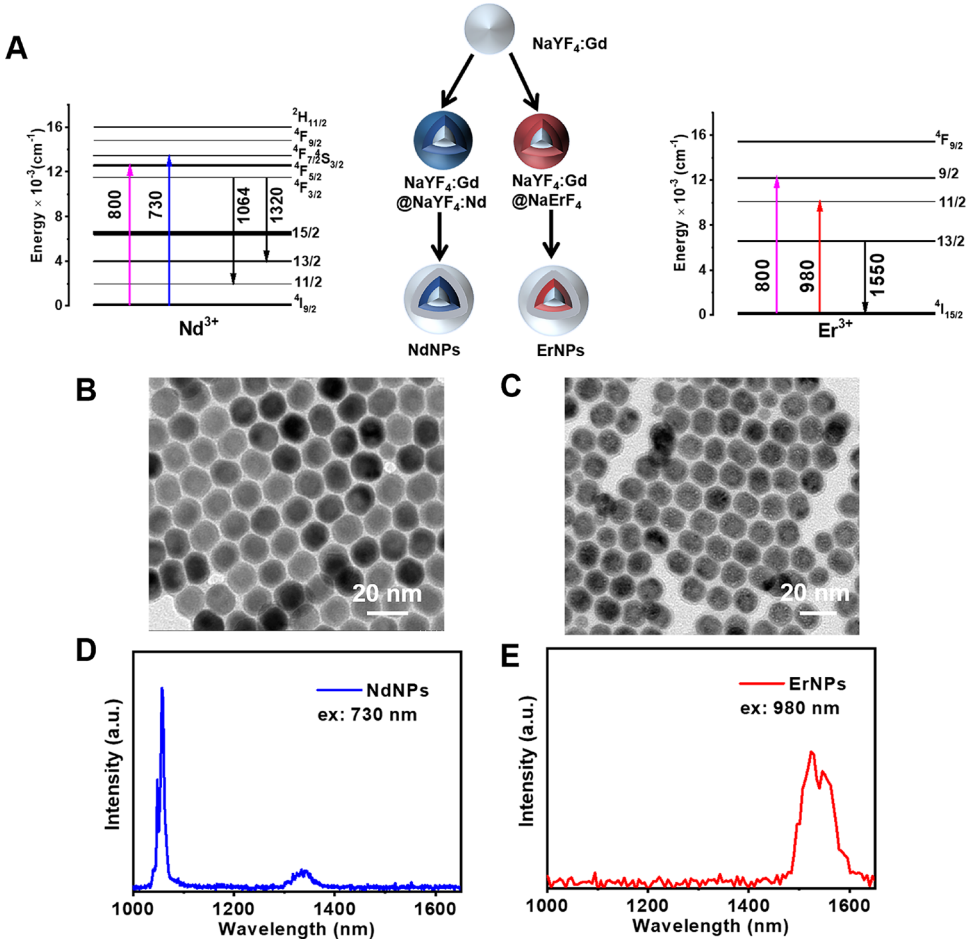

Figure 1. (A) Energy level diagram and the corresponding transition of Nd^{3+} and $Er^{3+}$and flow diagram of the synthesis of the core−shell−shell NdNPs and ErNPs. TEM images of (B) NdNPs and (C) ErNPs. NIR spectra of NdNPs and ErNPs excited using (D) 730 nm and (E) 980 nm lasers, respectively.

distribution of ∼27 nm (Figure 1B,C and Figure S1). The energy-dispersive X-ray analysis and the powder X-ray diffraction patterns confirm the as-designed chemical composition and hexagonal crystal phase of NdNPs and ErNPs, respectively (Figures S2 and S3). After coating the inert shell, their emissions were significantly enhanced because of the protection of the photoluminescence layer by the second inert shell (Figure S4). The upconversion luminescence (UCL) spectra and UCL images of $NaYF_4$:Gd@$NaErF_4$ and ErNPs also support the protection of the photoluminescence layer by the $NaYF_4$ shell (Figure S5). The $^4F_{3/2} \rightarrow {}^4I_{11/2}$ and $^4F_{3/2} \rightarrow {}^4I_{13/2}$ of Nd^{3+} endow NdNPs with two sharp emission peaks centered at 1064 and 1330 nm in the second near-infrared window (NIR-II) under 730 nm excitation, while the $^4I_{13/2} \rightarrow {}^4I_{15/2}$ of Er^{3+} contributes to the 1550 nm emission of ErNPs under 980 nm excitation (Figure 1A). Therefore, by manipulating the excitation wavelengths and using appropriate filters, the fluorescence signal at different wavelengths could be selectively collected, which forms multiple fluorescence channels for information storage.

Based on the absorbance and emission spectra of NdNPs and ErNPs (Figure S6 and Figure 1D,E), a series of excitation-filter combinations are optimized to selectively collect fluorescence signals at a specific wavelength (Figure 2A). Under 730 nm irradiation, only NdNPs are excited, and thereby, the fluorescence at 1064 and 1330 nm could be simultaneously collected by using a 1000 nm long-pass filter (Figure 2B). Similarly, the 1550 nm fluorescence of ErNPs could be collected by a 1250 nm long-pass filter under the specific 980 nm irradiation (Figure 2C). Notably, when using an 800 nm laser as an excitation resource, due to their overlapped absorbance peak, the two emission peaks of NdNPs and one peak of ErNPs could be collected (Figure 2D). The signal intensity of NdNPs and ErNPs was weaker using 800 nm laser than that from 730 or 980 nm laser (Figure S7). The above results are confirmed not only by the spectra but by the fluorescence images, which indicate that our excitation-filter combination would be applicable for fluorescence imaging as well.

To further demonstrate the applicability of information storage using the as-designed nanoprobes and method, information storage and fluorescence imaging-based readout are performed in vitro. The binary number combinations ″1−0−1″, ″0−1−1″, and ″1−1−1″ are stored in separate 730-, 980-, and 800-excited NIR-II fluorescence channels corresponding to the on−off signals collected by the charge-coupled device (Figure 3A and Figure S8). It is noticed that the signal difference is sharp between ″1″ and ″0″, where a broad threshold could be applied to translate the information from the collected signals (Figure 3B). These results illustrate the possibility of information storage in different NIR-II fluorescence channels, which motivated us to perform the

https://doi.org/10.1021/acsanm.2c03951
ACS Appl. Nano Mater. XXXX, XXX, XXX−XXX

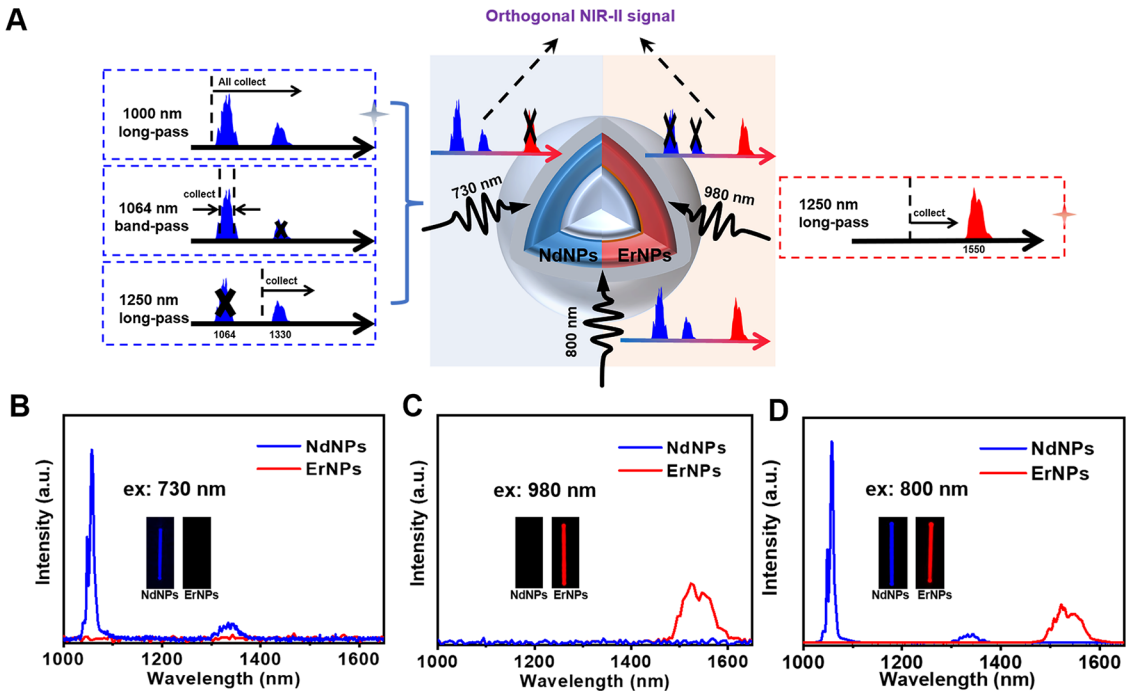

Figure 2. (A) Schematic diagram of collecting optimal NIR-II optical signal readout of NdNPs and ErNPs with a series of excitation-filter combinations. NIR spectra and (inset) NIR pseudo-color images of NdNPs and ErNPs excited by (B) 730 nm, (C) 980 nm, and (D) 800 nm laser, respectively.

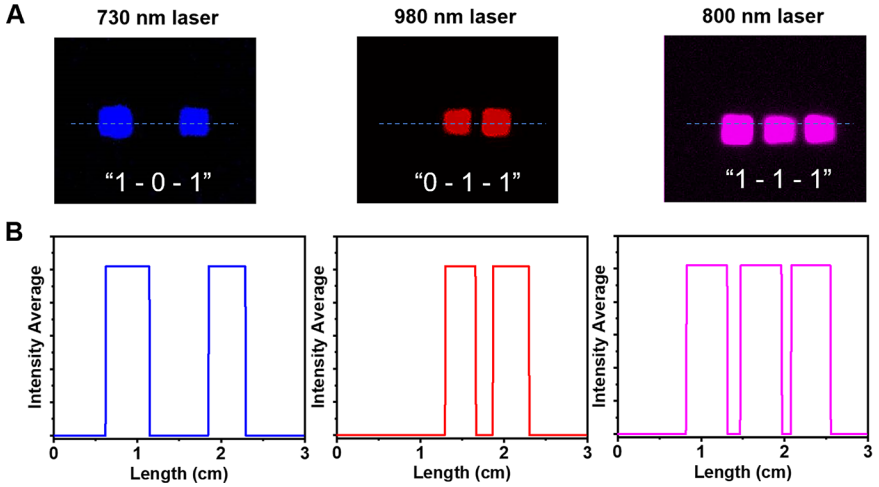

Figure 3. (A) NIR pseudo-color images of a 1 × 3 array containing NdNPs, ErNPs, and the mixture of NdNPs and ErNPs excited by 730, 980, and 800 nm laser by only filtering the incident light; the binary number combinations ″1−0−1″, ″0−1−1″, and ″1−1−1″ are stored in separate 730-, 980-, and 800-excited NIR-II fluorescence channels. (B) Averaged fluorescence intensity of the corresponding line position.

small-animal experiment by using the mice model. Hydrophilic $NaYF_4$:Gd@$NaYF_4$:Nd@$NaYF_4$-PEG (NdNPs-PEG) and $NaYF_4$:Gd@$NaErF_4$@$NaYF_4$-PEG (ErNPs-PEG) with no significant cytotoxicity to cells were constructed (Figure S9). The luminescence spectra of hydrophilic NdNPs-PEG and ErNPs-PEG showed that the fluorescence intensity of hydrophilic NdNPs-PEG and ErNPs-PEG was weaker than OA-capped NdNPs and OA-capped ErNPs. Additionally, the NIR-II signal intensities were positively correlated with its concentration (Figure S10). Upon in situ injection, the same binary number combinations were implanted under the mice's skin (Figure 4A). Similar results were observed as the in vitro experiment, which could contribute to the high penetration of NIR-II fluorescence in tissues. The signals ″on″ and ″off″, corresponding to ″1″ and ″0″, respectively, could be sharply identified from the fluorescence images (Figure 4B).

CONCLUSIONS

In summary, an *in vivo* information storage method is proposed based on a pair of lanthanide-doped nanoprobes (~27 nm) and is confirmed in the small-animal model by in situ implantation. From a perspective, more fluorescence channels could be introduced to store multiple different information *in vivo*. Also, optical devices could be established based on this strategy as implantation for complex information storage, and machine learning technology could be applied to identify and process. *In vivo* information storage based on lanthanum-

https://doi.org/10.1021/acsanm.2c03951
ACS Appl. Nano Mater. XXXX, XXX, XXX−XXX

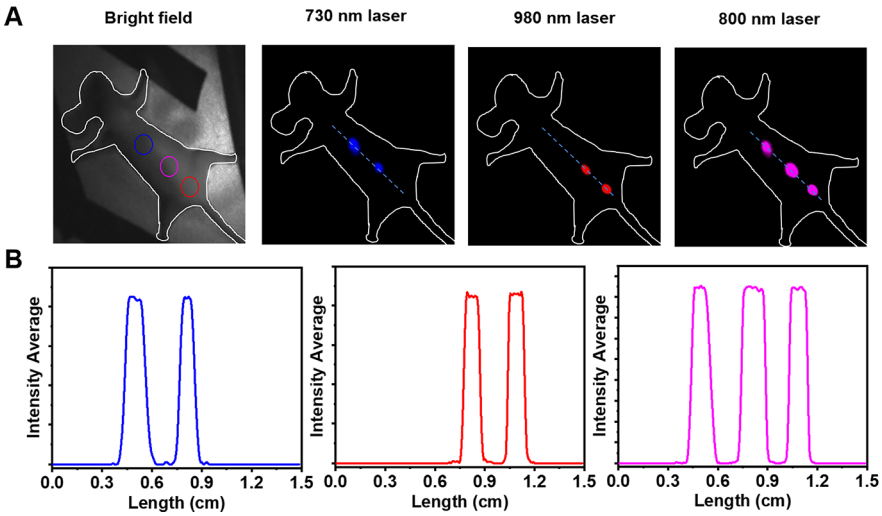

Figure 4. (A) Bright field image of the nude mouse. NdNPs-PEG, the mixture of NdNPs-PEG and ErNPs-PEG, and ErNPs-PEG aqueous dispersion were subcutaneously injected into the marked blue, pink, and red position, respectively. NIR pseudo-color images under the excitation of 730, 980, and 800 nm laser. The binary number combinations are implanted under the mice's skin. (B) Averaged fluorescence intensity of the corresponding line position.

doped nanoprobes has broad application prospects and promotes the development of photonics.

EXPERIMENTAL SECTION

The Synthesis of $NaYF_4$:Gd@$NaYF_4$:Nd@$NaYF_4$ and $NaYF_4$:Gd@$NaErF_4$@$NaYF_4$ Nanoparticles. The $NaYF_4$:Gd, $NaYF_4$:Gd@$NaYF_4$:Nd, $NaYF_4$:Gd@$NaErF_4$, $NaYF_4$:Gd@$NaYF_4$:Nd@$NaYF_4$ (NdNPs), and $NaYF_4$:Gd@$NaErF_4$@$NaYF_4$ (ErNPs) nanoparticles were synthesized according to the previously reported solvothermal method. For details, please see the Supporting Information.

The Synthesis of $NaYF_4$:Gd@$NaYF_4$:Nd@$NaYF_4$-PEG and $NaYF_4$:Gd@$NaErF_4$@$NaYF_4$-PEG Nanoparticles. NdNPs dispersed in 0.5 mL of cyclohexane were deposited by adding 6 mL of ethanol. The NdNPs were dispersed in 2 mL of $CHCl_3$ into a round-bottomed flask after centrifugation. Then, 6.2 mg of DSPE-m-PEG-2000 and 2.7 mg of DSPC were added into the round-bottomed flask. The $CHCl_3$ was removed by a rotary evaporator at 50 °C for 5 min, and then 2 mL of deionized water was injected and stirred for 1 h. After centrifugation and dispersing in 2 mL of deionized water, $NaYF_4$:Gd@$NaYF_4$:Nd@$NaYF_4$-PEG (NdNPs-PEG) was obtained. The synthesis of hydrophilic $NaYF_4$:Gd@$NaErF_4$@$NaYF_4$-PEG (ErNPs-PEG) was similar to that of NdNPs-PEG.

Optical Properties of the Synthesized Nanoparticles. NIR-II spectra of all synthesized nanoparticles were collected using 800 nm laser (240 mW), 730 nm laser (240 mW), and 980 nm laser (230 mW). The activator concentrations of all nanoparticles were 0.03 mmol unless otherwise specified, and the slit width was 1 nm during the spectral test unless otherwise specified.

NIR Imaging In Vivo. The nude mouse (body weight was about 20 g), which was subcutaneously injected NdNPs-PEG, the mixture of NdNPs-PEG and ErNPs-PEG, ErNPs-PEG aqueous dispersion (100 μL, 10 mg mL^{-1}) into up, middle, and down positions, which were marked with the circle, was anesthetized with 100 μL of 1% pentobarbital sodium salt aqueous solution by intraperitoneal injection for the following multicolor imaging. The bright field image was collected by NIR CCD within ambient light, and the NIR-II imaging photos were recorded by NIR CCD under the irradiation of 730, 980, and 800 nm laser, respectively.

ASSOCIATED CONTENT

Supporting Information

The Supporting Information is available free of charge at https://pubs.acs.org/doi/10.1021/acsanm.2c03951.

Experimental details, materials, and methods, including photographs of particle size distribution, EDXA spectra, PXRD pattern, and additional figures (PDF)

AUTHOR INFORMATION

Corresponding Author

Jing Zhou − *Beijing Key Laboratory for Optical Materials and Photonic Devices & Department of Chemistry, Capital Normal University, 100048 Beijing, China;* orcid.org/0000-0002-5348-1966; Email: jingzhou@cnu.edu.cn

Authors

Xiaolu Wang − *Beijing Key Laboratory for Optical Materials and Photonic Devices & Department of Chemistry, Capital Normal University, 100048 Beijing, China*

Qi Jia − *Beijing Key Laboratory for Optical Materials and Photonic Devices & Department of Chemistry, Capital Normal University, 100048 Beijing, China; Department of Biotechnology, Delft University of Technology, 2629 HZ, Delft, The Netherlands*

Liyi Ma − *Beijing Key Laboratory for Optical Materials and Photonic Devices & Department of Chemistry, Capital Normal University, 100048 Beijing, China; Key Laboratory of Photochemical Conversion and Optoelectronic Materials, Technical Institute of Physics and Chemistry, Chinese Academy of Sciences, Beijing 100190, People's Republic of China*

Xuejiao Zhai − *Beijing Key Laboratory for Optical Materials and Photonic Devices & Department of Chemistry, Capital Normal University, 100048 Beijing, China*

Yuxin Liu − *Beijing Key Laboratory for Optical Materials and Photonic Devices & Department of Chemistry, Capital Normal University, 100048 Beijing, China; Department of Biomolecular System, Max-Planck Institute for Colloids and Interfaces, 14476 Potsdam, Germany*

https://doi.org/10.1021/acsanm.2c03951
ACS Appl. Nano Mater. XXXX, XXX, XXX−XXX

Xianquan Liao − *Beijing Key Laboratory for Optical Materials and Photonic Devices & Department of Chemistry, Capital Normal University, 100048 Beijing, China*

Complete contact information is available at: https://pubs.acs.org/10.1021/acsanm.2c03951

Author Contributions

⊥X.W. and Q.J. contributed equally to this work.

Notes

The authors declare no competing financial interest.

■ ACKNOWLEDGMENTS

The authors would like to acknowledge the financial support from the National Natural Science Foundation of China (92159103), Beijing Municipal Education Commission Outstanding Young Individual Project (CIT&TCD201904082), Youth High-level Talent Project of Capital Normal University (20530810024), and Yanjing Young Scholar Program of Capital Normal University.

■ REFERENCES

(1) Carnicer, A.; Javidi, B. Optical Security and Authentication Using Nanoscale and Thin-Film Structures. *Adv. Opt. Photonics* **2017**, *9*, 218.

(2) Fan, Y.; Zhang, C.; Gao, Z.; Zhou, W.; Hou, Y.; Zhou, Z.; Yao, J.; Zhao, Y. S. Randomly Induced Phase Transformation in Silk Protein-Based Microlaser Arrays for Anticounterfeiting. *Adv. Mater.* **2021**, *33*, 2102586.

(3) Ma, J.; Li, Y.; Hu, W.; Wang, W.; Zhang, J.; Yang, J.; Wang, Y. A Terbium Activated Multicolour Photoluminescent Phosphor for Luminescent Anticounterfeiting. *J. Rare Earths* **2020**, *38*, 1039−1043.

(4) Pan, S.; Zhu, M. Fiber Electronics Bring a New Generation of Acoustic Fabrics. *Adv. Fiber Mater.* **2022**, *4*, 321−323.

(5) Nagarkar, A. A.; Root, S. E.; Fink, M. J.; Ten, A. S.; Cafferty, B. J.; Richardson, D. S.; Mrksich, M.; Whitesides, G. M. Storing and Reading Information in Mixtures of Fluorescent Molecules. *ACS Cent. Sci.* **2021**, *7*, 1728−1735.

(6) Zhuang, Y.; Lv, Y.; Wang, L.; Chen, W.; Zhou, T.-L.; Takeda, T.; Hirosaki, N.; Xie, R.-J. Trap Depth Engineering of $SrSi_2O_2N_2$:Ln^{2+}, Ln^{3+} (Ln^{2+} = Yb, Eu; Ln^{3+} = Dy, Ho, Er) Persistent Luminescence Materials for Information Storage Applications. *ACS Appl. Mater. Interfaces* **2018**, *10*, 1854−1864.

(7) Dien, V. T.; Holcomb, M.; Feldman, A. W.; Fischer, E. C.; Dwyer, T. J.; Romesberg, F. E. Progress Toward a Semi-Synthetic Organism with an Unrestricted Expanded Genetic Alphabet. *J. Am. Chem. Soc.* **2018**, *140*, 16115−16123.

(8) Zhuang, Y.; Chen, D.; Chen, W.; Zhang, W.; Su, X.; Deng, R.; An, Z.; Chen, H.; Xie, R.-J. X-Ray-Charged Bright Persistent Luminescence in $NaYF_4$:Ln^{3+}@$NaYF_4$ Nanoparticles for Multidimensional Optical Information Storage. *Light: Sci. Appl.* **2021**, *10*, 132.

(9) Nimi, N.; Saraswathy, A.; Nazeer, S. S.; Francis, N.; Shenoy, S. J.; Jayasree, R. S. Multifunctional Hybrid Nanoconstruct of Zerovalent Iron and Carbon Dots for Magnetic Resonance Angiography and Optical Imaging: An In Vivo Study. *Biomaterials* **2018**, *171*, 46−56.

(10) Poß, M.; Tower, R. J.; Napp, J.; Appold, L. C.; Lammers, T.; Alves, F.; Glüer, C.-C.; Boretius, S.; Feldmann, C. Multimodal $[GdO]^+$ $[ICG]^-$ Nanoparticles for Optical, Photoacoustic, and Magnetic Resonance Imaging. *Chem. Mater.* **2017**, *29*, 3547−3554.

(11) Aziz, A.; Holthof, J.; Meyer, S.; Schmidt, O. G.; Medina-Sánchez, M. Dual Ultrasound and Photoacoustic Tracking of Magnetically Driven Micromotors: From In Vitro to In Vivo. *Adv. Healthcare Mater.* **2021**, *10*, 2101077.

(12) Yang, F.; Skripka, A.; Benayas, A.; Dong, X.; Hong, S. H.; Ren, F.; Oh, J. K.; Liu, X.; Vetrone, F.; Ma, D. An Integrated Multifunctional Nanoplatform for Deep-Tissue Dual-Mode Imaging. *Adv. Funct. Mater.* **2018**, *28*, 1706235.

(13) Litti, L.; Rivato, N.; Fracasso, G.; Bontempi, P.; Nicolato, E.; Marzola, P.; Venzo, A.; Colombatti, M.; Gobbo, M.; Meneghetti, M. A SERRS/MRI Multimodal Contrast Agent Based on Naked Au Nanoparticles Functionalized with a Gd(III) Loaded PEG Polymer for Tumor Imaging and Localized Hyperthermia. *Nanoscale* **2018**, *10*, 1272−1278.

(14) Desai, M.; Slusarczyk, A. L.; Chapin, A.; Barch, M.; Jasanoff, A. Molecular Imaging with Engineered Physiology. *Nat. Commun.* **2016**, *7*, 13607.

(15) Hai, J.; Li, T.; Su, J.; Liu, W.; Ju, Y.; Wang, B.; Hou, Y. Reversible Response of Luminescent Terbium (III)-Nanocellulose Hydrogels to Anions for Latent Fingerprint Detection and Encryption. *Angew. Chem., Int. Ed.* **2018**, *57*, 6786−6790.

(16) Liu, H.; Li, J.; Hu, P.; Sun, S.; Shi, L.; Sun, L. Facile Synthesis of Er^{3+}/Tm^{3+} Co-Doped Magnetic/Luminescent Nanosystems for Possible Bioimaging and Therapy Applications. *J. Rare Earths* **2022**, *40*, 11−19.

(17) Xie, Y.; Chen, Q.; Wang, M.; Chen, W.; Quan, Z.; Li, C. Highly Doped NaErF4-Based Nanocrystals for Multi-Tasking Application. *J. Rare Earths* **2021**, *39*, 1467−1476.

(18) Abe, I.; Hara, M.; Seki, T.; Cho, S. J.; Shimizu, M.; Matsuura, K.; Cheong, H.-K.; Kim, J. Y.; Oh, J.; Jung, J.; Han, M. A Trigonal Molecular Assembly System with the Dual Light-Driven Functions of Phase Transition and Fluorescence Switching. *J. Mater. Chem. C* **2019**, *7*, 2276−2282.

(19) Niu, Y.; Li, S.; Zhang, J.; Wan, W.; He, Z.; Liu, J.; Liu, K.; Ren, S.; Ge, L.; Du, X.; Gu, Z. Static−Dynamic Fluorescence Patterns Based on Photodynamic Disulfide Reactions for Versatile Information Storage. *Small* **2021**, *17*, 2102224.

(20) Zhang, H.; Fan, Y.; Pei, P.; Sun, C.; Lu, L.; Zhang, F. Tm^{3+}-Sensitized NIR-II Fluorescent Nanocrystals for In Vivo Information Storage and Decoding. *Angew. Chem., Int. Ed.* **2019**, *58*, 10153−10157.

(21) Zhu, Q. Y.; Zhang, F. R.; Du, Y.; Zhang, X. X.; Lu, J. Y.; Yao, Q. F.; Huang, W. T.; Ding, X. Z.; Xia, L. Q. Graphene-Based Steganographically Aptasensing System for Information Computing, Encryption and Hiding, Fluorescence Sensing and in Vivo Imaging of Fish Pathogens. *ACS Appl. Mater. Interfaces* **2019**, *11*, 8904−8914.

(22) Li, Z.; Liang, T.; Wang, Q.; Liu, Z. Strategies for Constructing Upconversion Luminescence Nanoprobes to Improve Signal Contrast. *Small* **2020**, *16*, 1905084.

(23) Labrador-Páez, L.; Kostiv, U.; Widengren, J.; Liu, H. Water: An Influential Agent for Lanthanide-Doped Luminescent Nanoparticles in Nanomedicine. *Adv. Opt. Mater.* **2022**, 2200513.

(24) Zhai, X.; Song, B.; Chu, B.; Su, Y.; Wang, H.; He, Y. Highly Fluorescent, Photostable, and Biocompatible Silicon Theranostic Nanoprobes against Staphylococcus Aureus Infections. *Nano Res.* **2018**, *11*, 6417−6427.

(25) Zhang, M.; Zheng, W.; Liu, Y.; Huang, P.; Gong, Z.; Wei, J.; Gao, Y.; Zhou, S.; Li, X.; Chen, X. A New Class of Blue-LED-Excitable NIR-II Luminescent Nanoprobes Based on Lanthanide-Doped CaS Nanoparticles. *Angew. Chem., Int. Ed.* **2019**, *58*, 9556−9560.

(26) Tu, D.; Zheng, W.; Liu, Y.; Zhu, H.; Chen, X. Luminescent Biodetection Based on Lanthanide-Doped Inorganic Nanoprobes. *Coord. Chem. Rev.* **2014**, *273*−*274*, 13−29.

(27) Shen, C.; Gao, M.; Chen, H.; Zhan, Y.; Lan, Q.; Li, Z.; Xiong, W.; Qin, Z.; Zheng, L.; Zhao, J. Reactive Oxygen Species (ROS)-Responsive Nanoprobe for Bioimaging and Targeting Therapy of Osteoarthritis. *J. Nanobiotechnol.* **2021**, *19*, 395.

(28) Jin, J.; Gu, Y.-J.; Man, C. W.-Y.; Cheng, J.; Xu, Z.; Zhang, Y.; Wang, H.; Lee, V. H.-Y.; Cheng, S. H.; Wong, W.-T. Polymer-Coated $NaYF_4$:Yb^{3+}, Er^{3+} Upconversion Nanoparticles for Charge-Dependent Cellular Imaging. *ACS Nano* **2011**, *5*, 7838−7847.

(29) Zuo, M.; Duan, Q.; Li, C.; Ge, J.; Wang, Q.; Li, Z.; Liu, Z. A Versatile Strategy for Constructing Ratiometric Upconversion Luminescent Probe with Sensitized Emission of Energy Acceptor. *Anal. Chem.* **2021**, *93*, 5635−5643.

(30) Xu, J.; Gulzar, A.; Yang, P.; Bi, H.; Yang, D.; Gai, S.; He, F.; Lin, J.; Xing, B.; Jin, D. Recent Advances in Near-Infrared Emitting Lanthanide-Doped Nanoconstructs: Mechanism, Design and Application for Bioimaging. *Coord. Chem. Rev.* **2019**, *381*, 104−134.
(31) Xie, Y.; Song, Y.; Sun, G.; Hu, P.; Bednarkiewicz, A.; Sun, L. Lanthanide-Doped Heterostructured Nanocomposites toward Advanced Optical Anti-Counterfeiting and Information Storage. *Light: Sci. Appl.* **2022**, *11*, 150.
(32) Lee, J.; Yoo, B.; Lee, H.; Cha, G. D.; Lee, H.-S.; Cho, Y.; Kim, S. Y.; Seo, H.; Lee, W.; Son, D.; Kang, M.; Kim, H. M.; Park, Y. I.; Hyeon, T.; Kim, D.-H. Ultra-Wideband Multi-Dye-Sensitized Upconverting Nanoparticles for Information Security Application. *Adv. Mater.* **2017**, *29*, 1603169.
(33) Liu, X.; Wang, Y.; Li, X.; Yi, Z.; Deng, R.; Liang, L.; Xie, X.; Loong, D. T. B.; Song, S.; Fan, D.; All, A. H.; Zhang, H.; Huang, L.; Liu, X. Binary Temporal Upconversion Codes of Mn^{2+}-Activated Nanoparticles for Multilevel Anti-Counterfeiting. *Nat. Commun.* **2017**, *8*, 899.
(34) Hasegawa, Y.; Kitagawa, Y. Luminescent Lanthanide Coordination Polymers with Transformative Energy Transfer Processes for Physical and Chemical Sensing Applications. *J. Photochem. Photobiol., C* **2022**, *51*, 100485.
(35) Hasegawa, Y.; Kitagawa, Y. Thermo-Sensitive Luminescence of Lanthanide Complexes, Clusters, Coordination Polymers and Metal−Organic Frameworks with Organic Photosensitizers. *J. Mater. Chem. C* **2019**, *7*, 7494−7511.
(36) Huang, J.; Yan, L.; Liu, S.; Song, N.; Zhang, Q.; Zhou, B. Dynamic Control of Orthogonal Upconversion in Migratory Core−Shell Nanostructure toward Information Security. *Adv. Funct. Mater.* **2021**, *31*, 2009796.
(37) Zhu, Y.; Zhao, J.; Li, X.; Xu, X.; Huang, J.; Ji, X.; Yang, G.; Pan, G. Stable and Efficient Upconversion Single Red Emission from $CsPbI_3$ Perovskite Quantum Dots Triggered by Upconversion Nanoparticles. *Inorg. Chem.* **2021**, *60*, 2649−2655.
(38) Gu, Y.; Guo, Z.; Yuan, W.; Kong, M.; Liu, Y.; Liu, Y.; Gao, Y.; Feng, W.; Wang, F.; Zhou, J.; Jin, D.; Li, F. High-Sensitivity Imaging of Time-Domain near-Infrared Light Transducer. *Nat. Photonics* **2019**, *13*, 525−531.
(39) Fan, Y.; Wang, P.; Lu, Y.; Wang, R.; Zhou, L.; Zheng, X.; Li, X.; Piper, J. A.; Zhang, F. Lifetime-engineered NIR-II nanoparticles unlock multiplexed in vivo imaging. *Nat. Nanotechnol.* **2018**, *13*, 941−946.
(40) Ortgies, D. H.; Tan, M.; Ximendes, E. C.; del Rosal, B.; Hu, J.; Xu, L.; Wang, X.; Martín Rodríguez, E.; Jacinto, C.; Fernandez, N.; Chen, G.; Jaque, D. Lifetime-Encoded Infrared-Emitting Nanoparticles for in Vivo Multiplexed Imaging. *ACS Nano* **2018**, *12*, 4362−4368.
(41) Liang, T.; Guo, Z.; He, Y.; Wang, Y.; Li, C.; Li, Z.; Liu, Z. Cyanine-Doped Lanthanide Metal-Organic Frameworks for Near-Infrared II Bioimaging. *Adv. Sci.* **2022**, *9*, No. e2104561.
(42) Jia, Q.; Ma, L.; Zhai, X.; Fu, W.; Liu, Y.; Liao, X.; Zhou, J. Orthogonal Near-Infrared-II Imaging Enables Spatially Distinguishing Tissues Based on Lanthanide-Doped Nanoprobes. *Anal. Chem.* **2020**, *92*, 14762−14768.
(43) Ma, B. L.; Zhai, X.; Du, G.; Zhou, J. Orthogonal Shortwave Infrared Emission Based on Rare Earth Nanoparticles for Interference-Free Logical Codes and Bio-Imaging. *Chem. Sci.* **2019**, *10*, 3281−3288.

https://doi.org/10.1021/acsanm.2c03951
ACS Appl. Nano Mater. XXXX, XXX, XXX−XXX